

ChimeraLM: a language model enables accurate  
structural variant detection in whole-genome  
amplified long-read sequencing

Yangyang Li<sup>1†</sup>, Qingxiang Guo<sup>1†</sup>, Rendong Yang<sup>1,2\*</sup>

<sup>1</sup>Department of Urology, Northwestern University Feinberg School of Medicine, 303 E Superior St, Chicago, 60611, IL, USA.

<sup>2</sup>Robert H. Lurie Comprehensive Cancer Center, Northwestern University Feinberg School of Medicine, 675 N St Clair St, Chicago, 60611, IL, USA.

\*Corresponding author(s). E-mail(s): [rendong.yang@northwestern.edu](mailto:rendong.yang@northwestern.edu);  
Contributing authors: [yangyang.li@northwestern.edu](mailto:yangyang.li@northwestern.edu);

[qingxiang.guo@northwestern.edu](mailto:qingxiang.guo@northwestern.edu);

†These authors contributed equally to this work.

## Abstract

Single-cell genomic analysis relies on [whole genome amplification \(WGA\)](#) to generate sufficient DNA for sequencing, yet this process introduces chimera artifacts that manifest as false-positive [structural variation \(SV\)](#) and compromise downstream analyses. Here we present ChimeraLM, an interpretable [genomic language model \(GLM\)](#) that identifies [WGA](#)-induced chimera artifacts directly from sequence information. ChimeraLM is trained on matched [WGA](#) and bulk long-read sequencing from the same sample, using bulk support to label chimeric reads as amplification-induced artifacts or genuine genomic events. To capture long-range dependencies in variable-length reads, the model integrates Hyena operators with attention pooling. Evaluated on matched [WGA](#) and bulk nanopore datasets, ChimeraLM eliminated ~90% of chimeric reads from [WGA](#) data, restoring chimeric read proportion to near-bulk levels, whereas existing approaches achieved at most an 8% reduction. Using high-confidence [SV](#) call sets derived from matched bulk data as a reference, ChimeraLM removed 92-93% of unsupported [SV](#) calls from [WGA](#) datasets while retaining 72-92% of bulk-supported [SVs](#). ChimeraLM further normalized [SV](#) type distributions toward bulk profiles by suppressing the characteristic inversion bias observed in unprocessed [WGA](#) data. Attention-based interpretation indicates that ChimeraLM

047 concentrates classification evidence at chimeric junctions, demonstrating its ability  
048 to learn biologically interpretable features. ChimeraLM provides a general  
049 approach for suppressing amplification-induced artifacts, enabling more reliable  
050 single-cell **SV** analysis across long-read platforms.

051 **Keywords:** Whole Genome Amplification, Single Cell, Genomic Language Model,  
052 Structural Variation

## 056 Main

058 Single-cell and low-input genomics have transformed our ability to resolve biological  
059 heterogeneity, enabling the discovery of rare cell states and the reconstruction of clonal  
060 evolution in cancer and development [1–3]. However, the limited DNA input (on the  
061 order of picograms per cell) makes comprehensive genome-wide profiling technically  
062 challenging [4, 5]. **Whole genome amplification (WGA)** therefore remains a prerequisite  
063 for high-coverage sequencing [6–8], yet it introduces systematic errors that compromise  
064 genomic fidelity, particularly for **structural variation (SV)** detection [9–11].

065 A major source of error in **WGA** is amplification-induced chimera formation.  
066 During this process, highly processive polymerases such as phi29, which is used in  
067 **multiple displacement amplification (MDA)**, can switch templates and join discontinuous  
068 genomic loci into a single molecule [9–13]. As a result, **WGA**-based sequencing  
069 often produces chimeric reads that constitute a substantial fraction of the data [9].  
070 These artificial sequences frequently create alignment patterns that closely resemble  
071 those generated by genuine **SVs**, including **translocations (TRAs)** and **inversions (INVs)** [10]. Consequently, **SV** callers that rely on alignment-based signals (e.g., split-  
072 read and supplementary alignments) and coverage-derived evidence often misinterpret  
073 these amplification artifacts as true rearrangements, inflating false positives and distorting  
074 **SV** spectra [14–22]. This problem is particularly consequential for **WGA**-based  
075 long-read sequencing, which is otherwise well suited for resolving complex **SVs** at  
076 sing-cell resolution [23, 24].

077 Distinguishing genuine genomic rearrangements from **WGA**-induced chimera artifacts  
078 remains a major computational challenge. Existing quality-control approaches  
079 typically rely on handcrafted rules or alignment-derived features, such as read orientation  
080 signatures or local coverage deviations [11, 13, 25]. However, these heuristics  
081 are often sensitive to platform- and protocol-specific variation. Moreover, they cannot  
082 capture sequence-level patterns or long-range dependencies within reads. As a result,  
083 low-input long-read sequencing remains difficult to deploy in settings where high precision  
084 is essential, including somatic mosaicism profiling [26] and validation of CRISPR  
085 off-target effects [27].

086 To address this challenge, we present ChimeraLM, an interpretable **genomic language model (GLM)**  
087 for identifying and filtering **WGA**-induced artifacts at the single-read level. Unlike existing approaches that rely on handcrafted rules derived  
088 from read alignments or sequence-level [11, 13, 25], ChimeraLM formulates artifact  
089 detection as a sequence-modeling task and learns discriminative features directly from  
090

raw reads [28]. Building on advances in DNA foundation models [29–32], it captures latent motifs and structural dependencies that generalize across long-read sequencing platforms provided by Oxford Nanopore Technologies (ONT). On ONT WGA datasets, ChimeraLM reduces chimeric reads by ~90% while preserving 72–92% of bulk-supported SVs, improving SV validation rates by 8.5- to 11.0-fold and restoring bulk-like SV type distributions. Together, ChimeraLM provides an effective and interpretable filter for WGA long-read data, enabling robust SV discovery in single-cell and low-input genomics.

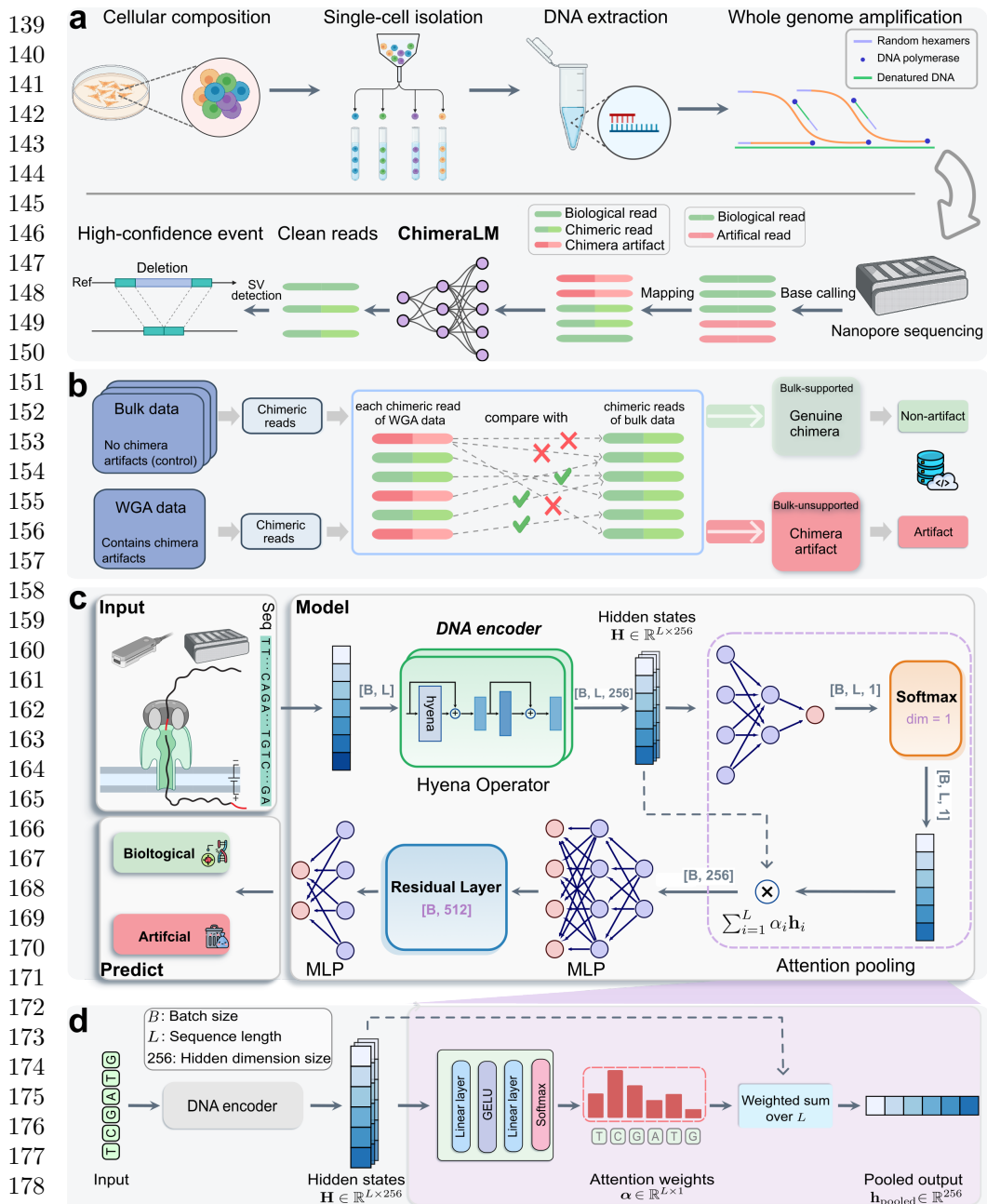
## Results

### Overview of ChimeraLM workflow and model architecture

ChimeraLM operates as a post-alignment filtering module within the single-cell long-read sequencing pipeline (Fig. 1a). After base calling and alignment to the reference genome, the resulting read set typically contains a mixture of true chimeric reads that arise from authentic genomic rearrangements and artificial chimeras introduced during WGA. ChimeraLM evaluates all reads with chimeric alignments before variant calling. For each read, the model determines whether the observed chimera reflects a genuine genomic event or a WGA-induced artifact. This binary classification enables selective removal of artificial chimeric reads while preserving true rearrangements, which improves the accuracy and sensitivity of downstream SV analyses.

To construct a robust supervised training set, we generated WGA long-read sequencing data from the human prostate cancer cell line PC3 using the ONT PromethION platform. For ground-truth calibration, we acquired three matched bulk long-read datasets from unamplified genomic DNA across diverse technologies: ONT PromethION, ONT MinION, and Pacific Biosciences (PacBio) Sequel II. Leveraging these references, we established a bulk-supported labeling framework by cross-referencing each WGA chimeric read against the chimeric alignment structures identified in the unamplified bulk data (Methods; Fig. 1b; Extended Data Fig. 1a). Under this classification scheme, WGA reads with alignment architectures corroborated by bulk evidence were labeled as genuine genomic events, while those lacking bulk support were classified as WGA-induced artifacts. To evaluate the model’s ability to generalize across sequencing hardware, we generated an independent WGA dataset on the MinION platform, which was reserved exclusively for testing (Extended Data Fig. 1a).

This labeling procedure classified 12,963,576 chimeric reads from the WGA PromethION dataset into two groups (genuine events and WGA-induced artifacts) based on bulk support (Extended Data Fig. 1b). Among these, 12,670,396 reads (97.7%) showed no matching alignment structures in any bulk dataset and were labeled as WGA-induced artifacts. The remaining 293,180 reads (2.3%) had matching structures in at least one bulk dataset, indicating they represent genuine genomic events rather than amplification artifacts, and were labeled as genuine chimeric reads. To construct a balanced training dataset, we retained all 293,180 genuine chimeric reads and randomly subsampled an equal number of WGA-induced artifacts. We further added 178,748 chimeric reads sampled from the bulk datasets to the genuine-event set, expanding the



181    **Fig. 1 ChimeraLM workflow and architecture for detecting WGA artifacts.** (a) Single-cell 182    genomic workflow and ChimeraLM integration. Single cells are isolated, followed by DNA extraction 183    and WGA. During amplification, WGA-induced chimeric artifacts (red) are generated alongside 184    genuine chimeric reads (green). After base calling and mapping, ChimeraLM classifies reads with 185    chimeric alignments as genuine events or WGA-induced artifacts, enabling downstream SV detection 186    on filtered data. (b) Bulk-supported label generation. Chimeric reads from WGA data are compared 187    against bulk sequencing from the same cell line. Reads with bulk-supported alignment structures 188    are labeled as genuine events (green); reads with no bulk match are labeled as WGA-induced artifacts (red). (c) ChimeraLM architecture. Input DNA sequences (batch size  $B$ , sequence length  $L$ ) are 189    tokenized at single-nucleotide resolution and encoded into hidden states  $\mathbf{H} \in \mathbb{R}^{L \times 256}$  through 190    DNA encoder (HyenaDNA [29]). Hyena operators capture long-range dependencies. Attention pooling 191    aggregates position-specific features, and multilayer perceptron (MLP) layers with residual connections 192    process pooled representations for binary classification of genuine events and WGA-induced 193    artifacts. (d) Attention pooling mechanism. Attention weights  $\alpha \in \mathbb{R}^{L \times 1}$  are computed through linear 194    layers with GELU activation and softmax normalization, assigning importance scores to each 195    position. The weighted sum produces a fixed-dimensional representation  $\mathbf{h}_{\text{pooled}} \in \mathbb{R}^{256}$ . Created 196    with BioRender.com.

diversity of bulk-supported chimeric alignment structures used for training. The final labeled dataset comprised 765,108 reads and was split into training (70%), validation (20%), and test (10%) sets using stratified sampling (Extended Data Fig. 1a). 185  
186  
187

To model these labeled reads, ChimeraLM must process long, variable-length DNA sequences at single-nucleotide resolution (Fig. 1c). We therefore built ChimeraLM on HyenaDNA [29], a genomic foundation model pre-trained on diverse DNA sequences. Each read is tokenized at nucleotide resolution and encoded by Hyena operators [33], which capture long-range sequence context without splitting the input. The encoder produces a sequence of hidden states across the full read. To obtain a fixed-length representation for classification, ChimeraLM uses an attention-pooling module that learns position-specific weights and computes a weighted sum over the hidden states (Fig. 1d). The pooled representation is then passed through residual MLP blocks, and a final softmax outputs the probability that a read reflects a genuine event versus a WGA-induced artifact. 188  
189  
190  
191  
192  
193  
194  
195  
196  
197  
198  
199  
200  
201  
202  
203  
204  
205  
206  
207  
208  
209  
210  
211  
212  
213  
214  
215  
216  
217  
218  
219  
220  
221  
222  
223  
224  
225  
226  
227  
228  
229  
230

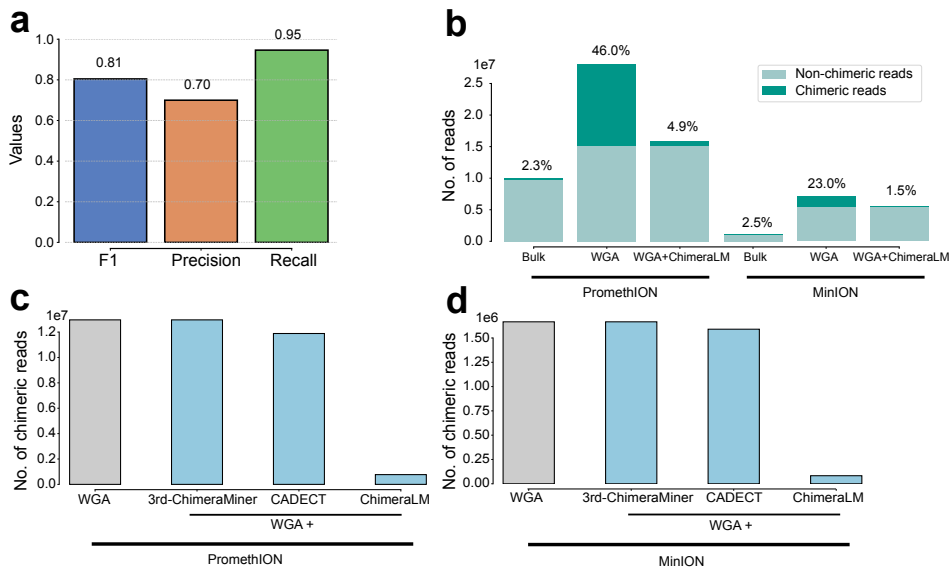


**Fig. 2 ChimeraLM accurately identifies and removes WGA-induced chimeric artifacts.** (a) Classification performance on held-out test data. ChimeraLM achieves recall of 0.95, precision of 0.70, and F1 score of 0.81. (b) Chimeric read reduction across sequencing platforms. Stacked bars show proportions of chimeric (dark teal) and non-chimeric (light teal) reads in bulk, WGA, and ChimeraLM-filtered samples. ChimeraLM reduces chimeric read frequencies from 46.0% to 4.9% (PromethION) and from 23.0% to 1.5% (MinION), approaching bulk levels (2.3% and 2.5%, respectively). (c,d) Benchmarking against existing methods on PromethION (c) and MinION (d). The gray bar indicates the total number of chimeric read on unfiltered WGA data. The blue bar represents the total number of chimeric reads remaining after filtering by each method. ChimeraLM achieves approximately 90% reduction in chimeric reads on both platforms, while 3rd-ChimeraMiner shows no detectable reduction and CADECT shows 8.3% and 4.6% reduction on PromethION and MinION, respectively. SACRA failed to complete due to memory exhaustion (> 500 GB RAM required).

231 **ChimeraLM achieves high accuracy and reduces artifacts to  
232 near-bulk levels across platforms**

233 We first benchmarked ChimeraLM using the held-out test split (10%) derived from  
234 the bulk-supported labeled dataset (Extended Data Fig. 1a). This test set consists of  
235 chimeric reads labeled as genuine events or **WGA**-induced artifacts based on whether  
236 their chimeric alignment structures are supported by matched bulk sequencing.  
237 ChimeraLM achieved an F1 score of 0.81, with 0.95 recall and 0.70 precision (Fig. 2a).  
238 The high recall indicates that most **WGA**-induced artifacts are correctly identified for  
239 removal, which is important for limiting downstream false-positive **SV** calls, while the  
240 precision confirms that most reads flagged as artifacts are true amplification-induced  
241 chimeras rather than genuine genomic events.  
242

243 We next examined whether applying ChimeraLM filtering would restore chimeric  
244 read rates in full PC3 **WGA** datasets toward the levels observed in bulk sequencing  
245 across both PromethION and MinION platforms (Fig. 2b). Bulk sequencing estab-  
246 lished low baseline chimeric read rates of 2.3% (PromethION) and 2.5% (MinION).  
247 In contrast, **WGA** increased the chimeric read fraction to 46.0% and 23.0%, respec-  
248 tively. After ChimeraLM filtering, chimeric content dropped to 4.9% on PromethION  
249 and 1.5% on MinION, corresponding to 10- to 15-fold reductions, while retaining 15.8  
250 million and 5.6 million reads. These post-filtering rates approach the corresponding  
251 bulk baselines, indicating effective removal of **WGA**-induced artifacts while preserving  
252 genuine signal.

253 We compared ChimeraLM against SACRA [25], 3rd-ChimeraMiner [13], and  
254 CADECT [11], existing tools for detecting amplification-induced chimeras (Fig. 2c,d).  
255 ChimeraLM reduced chimeric reads by ~90% on both platforms, substantially  
256 outperforming CADECT(8.3% and 4.6% reduction on PromethION and MinION,  
257 respectively), while 3rd-ChimeraMiner showed no detectable reduction. SACRA could  
258 not be evaluated due to out-of-memory errors even with 500 GB RAM.

259 The MinION results further provide an independent test of model generaliza-  
260 tion, as this MinION **WGA** dataset was not used during training. ChimeraLM was  
261 trained exclusively on PromethION **WGA** data, yet achieved comparable chimeric read  
262 reduction on MinION. This cross-platform generalization indicates that ChimeraLM  
263 captures sequence-level features intrinsic to **WGA**-induced artifacts rather than  
264 platform-specific signatures, supporting its potential applicability to additional long-  
265 read and potentially short-read sequencing technologies.

266  
267  
268  
269  
270  
271  
272  
273  
274  
275  
276

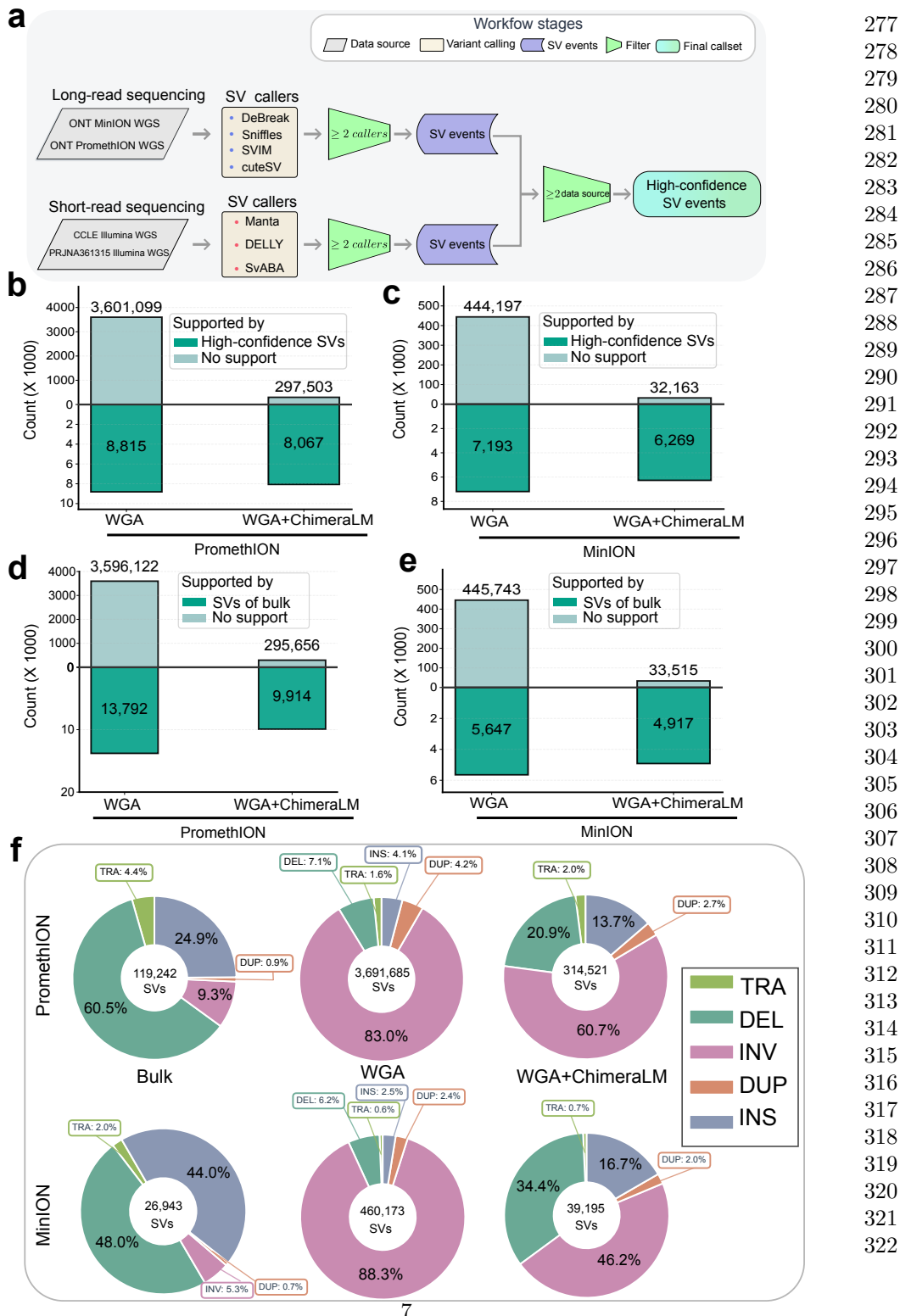


**Fig. 3 ChimeraLM improves structural variant detection accuracy.** (a) Construction of a high-confidence SV reference dataset from bulk PC3 sequencing. Four bulk datasets were integrated: ONT MinION Mk1C, ONT PromethION P2, the CCLE Illumina whole genome sequencing (WGS) dataset, and the PRJNA361315 Illumina WGS dataset. SVs were called independently within each dataset using multiple callers, and events supported by ≥2 callers per dataset were retained. SVs were then compared across datasets, and events observed in ≥2 of the four bulk datasets were designated as gold-standard SVs. (b,c) SV validation against the gold-standard reference for PromethION (b) and MinION (c). Bars show SV calls supported by the gold standard (dark teal) or unsupported (light teal). (d,e) SV validation against platform-matched long-read bulk sequencing for PromethION (d) and MinION (e), capturing true long-read SVs that may not be represented in the multi-platform reference. Bars show SV calls supported by the platform-matched long-read bulk data (dark teal) or unsupported (light teal). (f) SV type distributions for PromethION and MinION across bulk, unfiltered WGA, and WGA+ChimeraLM. Unfiltered WGA shows an excess of INVs, which is reduced after ChimeraLM filtering.

323 **ChimeraLM substantially reduces unsupported structural  
324 variant calls**

325 Accurate **SV** detection from single cells is essential for characterizing genomic diversity  
326 and disease mechanisms. However, **WGA**-induced chimeric artifacts can be misinter-  
327 preted as genuine **SVs**, potentially leading to incorrect biological inferences. To assess  
328 the impact of ChimeraLM on **SV** calling, we compared **SV** callsets generated from  
329 unfiltered **WGA** reads with those obtained after applying ChimeraLM filtering (**WGA**  
330 + ChimeraLM). Both callsets were evaluated against two complementary bulk-derived  
331 references: (i) a stringent gold-standard **SV** set derived from bulk PC3 DNA through  
332 cross-dataset consensus, and (ii) platform-matched long-read bulk **SV** callsets used as  
333 platform-specific references.

334 We first constructed a high-confidence gold-standard **SV** set from bulk PC3  
335 DNA by integrating four independent sequencing datasets: **ONT** PromethION, **ONT**  
336 MinION, and two Illumina short-read **WGS** datasets from the Cancer Cell Line  
337 Encyclopedia (CCLE Illumina **WGS** [34]) and from a previously published study  
338 (PRJNA361315 Illumina **WGS** [35]) (Fig. 3a; Extended Data Table 1). **SVs** were called  
339 separately within each dataset using multiple **SV** callers. Events supported by at least  
340 two callers within a dataset were retained, and only **SVs** observed in at least two of  
341 the four datasets were designated as gold-standard events.

342 Relative to this stringent gold standard, unfiltered **WGA** produced a large number  
343 of unsupported **SVs**. On PromethION, **WGA** yielded 3,601,099 **SV** calls, of which  
344 only 8,815 (0.24%) overlapped gold-standard events. After ChimeraLM filtering, total  
345 calls decreased to 305,570 (a 91.5% reduction) while retaining 8,067 gold-standard  
346 events (91.5% retention), increasing the validation rate to 2.64% (11-fold) (Fig. 3b).  
347 On MinION, total calls decreased from 451,390 to 38,432 (a 91.5% reduction), while  
348 gold-standard-supported events decreased from 7,193 to 6,269, corresponding to 87.2%  
349 retention. The validation rate increased from 1.59% to 16.3% (10-fold) (Fig. 3c).

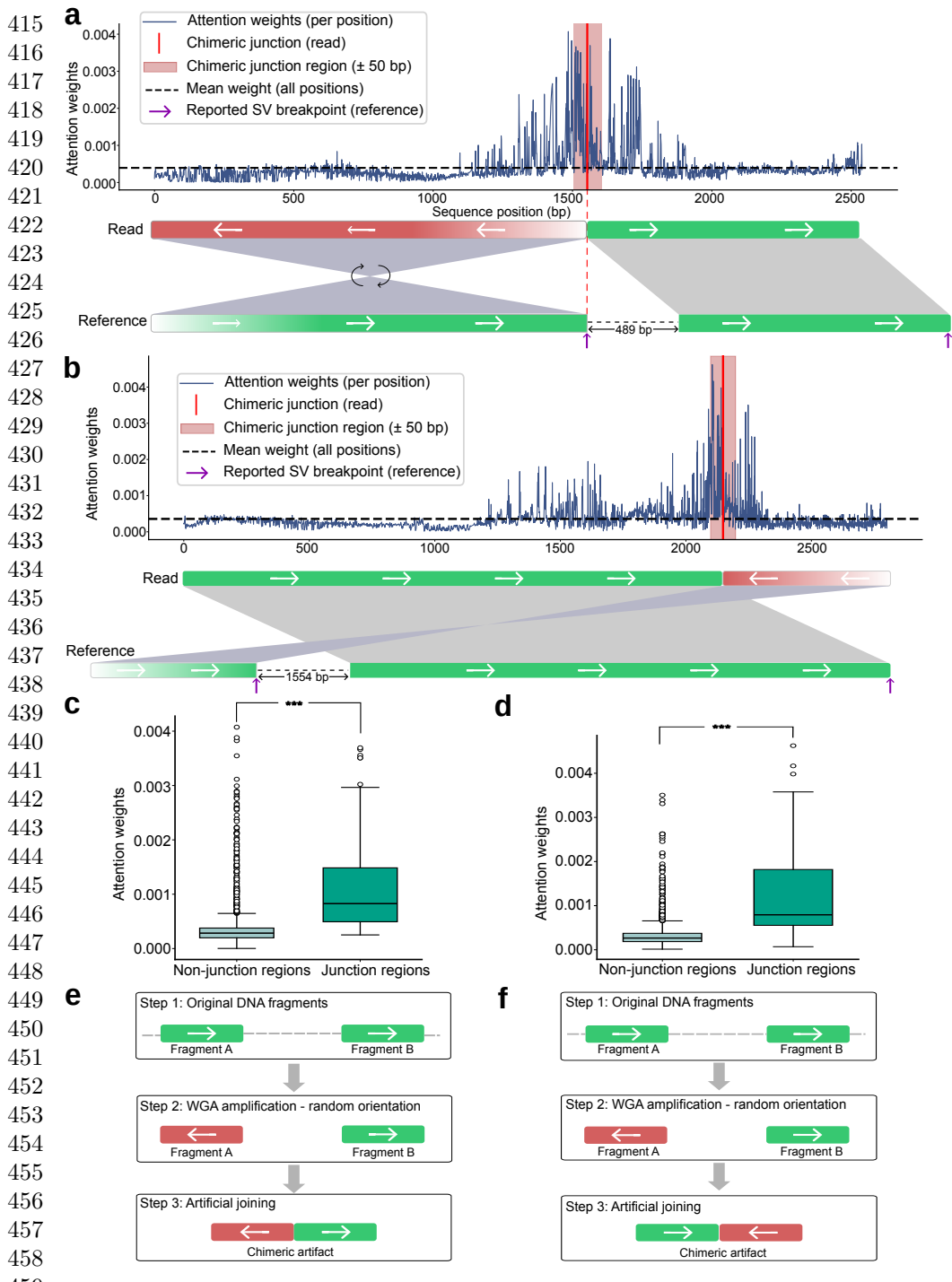
350 Because the gold standard is intentionally stringent and may exclude true **SVs**  
351 detectable only in long-read data, we next performed platform-matched validation  
352 using long-read bulk sequencing from the same platform (Fig. 3d,e). This analysis  
353 provides a platform-specific estimate of recall and reduces bias introduced by the  
354 strict gold-standard definition. ChimeraLM increased validation rates from 0.38% to  
355 3.24% on PromethION (8.5-fold) and from 1.25% to 12.79% on MinION (10-fold),  
356 while retaining 71.9% and 87.1% of bulk-supported events, respectively. Together,  
357 these results show that ChimeraLM removes the vast majority of unsupported **SV**  
358 calls while preserving the majority of bulk-supported variants across platforms.

360 **361 ChimeraLM mitigates WGA-induced SV type biases**

362 Amplification artifacts can distort the apparent spectrum of **SVs**. We therefore com-  
363 pared **SV** type compositions across bulk, unfiltered **WGA**, and ChimeraLM-filtered  
364 datasets on both nanopore platforms (Fig. 3f). Bulk sequencing showed a balanced  
365 mixture of **deletions (DELs)**, **duplications (DUPs)**, **insertions (INSSs)**, **INVs**, and **TRAs**.

In contrast, unfiltered **WGA** callsets were strongly enriched for **INVs**. ChimeraLM filtering reduced this excess, shifting the **SV**-type profile toward the bulk composition while leaving other **SV** classes comparatively stable. 369  
370  
371  
372  
373  
374  
375  
376  
377  
378  
379  
380  
381  
382  
383  
384  
385  
386  
387  
388  
389  
390  
391  
392  
393  
394  
395  
396  
397  
398  
399  
400  
401  
402  
403  
404  
405  
406  
407  
408  
409  
410  
411  
412  
413  
414

To determine which **SV** types were preferentially associated with amplification artifacts, we next examined **SV** calls supported exclusively by reads classified as **WGA**-induced artifacts (Extended Data Fig. 2). These artifact-supported events were dominated by **INVs**, accounting for 88.4% on PromethION and 92.4% on MinION. The remaining calls included smaller fractions of **DELs** (5.1% and 3.8%), **DUPs** (3.4% and 2.4%), and **INSs** (3.0% and 1.4%). Thus, **WGA**-induced artifacts primarily inflate **INV** calls, but also generate false positives across multiple **SV** categories. By selectively removing artifact-supported events, ChimeraLM restores **SV** type distributions toward bulk profiles, improving the accuracy and interpretability of single-cell **SV** analysis.



460 **Fig. 4 ChimeraLM attention weights are enriched at chimeric junction regions.**

(a,b) Attention weight profiles for two representative chimeric reads exhibiting distinct junction configurations. Upper panels show per-position attention weights (blue) with the mean attention across the read indicated by a dashed line. Red vertical lines mark inferred chimeric junction positions, and pink shading denotes the junction-centered region ( $\pm 50$  bp). Lower panels display read-level alignments, highlighting orientation transitions at the junctions (green, forward orientation; red, reverse-complemented orientation). (c,d) Quantitative comparison of attention weights between junction and non-junction regions. Junction-centered windows show significantly elevated attention weights relative to non-junction regions ( $P = 5.3 \times 10^{-14}$  and  $P = 6.8 \times 10^{-15}$ ; Wilcoxon rank-sum test). (e,f) Schematic illustration of WGA-induced chimera formation. During amplification, DNA fragments originating from distant genomic loci can be amplified in either orientation, joining them into a single molecule with discordant orientations, producing INV-like alignment signatures. The two examples illustrate forward-to-reverse and reverse-to-forward orientation transitions.

<b>Attention visualization reveals interpretable classification features</b>	461
	462
	463
	464
	465
	466
	467
	468
	469
	470
	471
	472
	473
	474
	475
	476
	477
	478
	479
	480
	481
	482
	483
	484
	485
	486
	487
	488
	489
	490
	491
	492
	493
	494
	495
	496
	497
	498
	499
	500
	501
	502
	503
	504
	505
	506
<b>WGA</b> enables genomic analysis from single cells and other low-input samples, but it also introduces chimeric artifacts that compromise <b>SV</b> detection. ChimeraLM addresses this challenge by classifying chimeric reads as genuine events or <b>WGA</b> -induced artifacts directly from read information, and removing artifacts before variant calling, rather than attempting to correct artifact-driven calls post hoc. Across <b>ONT</b> platforms, ChimeraLM improved data quality at the read and variant levels: it reduced chimeric reads by ~90% while retaining 72–92% of bulk-supported <b>SVs</b> , and it increased the ratio of supported <b>SV</b> calls by 8.5–11.0-fold. Notably, performance generalized from PromethION (used for training) to MinION without platform-specific retraining, suggesting that ChimeraLM captures properties shared by <b>WGA</b> -induced artifacts rather than instrument-specific signatures.	486
In comparison, existing methods showed limited effectiveness on our <b>ONT WGA</b> datasets. Two tools originally developed and primarily evaluated on PacBio data (SACRA and 3rd-ChimeraMiner) [13, 25] either failed to complete under our evaluation setting (SACRA, > 500 GB RAM) or showed no detectable reduction (3rd-ChimeraMiner), highlighting poor cross-platform generalization. CADECT [11], which was designed for <b>ONT</b> data, achieved only 8.3% and 4.6% reduction on PromethION and MinION, respectively. CADECT detects concatemers via sliding-window self-alignment, an effective strategy for repeat-like structures with internal sequence similarity, but it is not designed to capture the broader diversity of <b>WGA</b> -induced chimeras. Together, these comparisons suggest that rule-based or subtype-specific	487

507 heuristics do not comprehensively address amplification-induced chimeras and moti-  
508 vate learning-based models that can extract discriminative sequence signatures  
509 without imposing predefined structural assumptions.

510 ChimeraLM also illustrates the value of deep learning for quality-control problems  
511 where conventional alignment- and coverage-derived criteria provide limited resolu-  
512 tion. [11, 13, 25, 28]. By learning directly from sequence, ChimeraLM discovers subtle  
513 compositional and structural features that separate genuine events from amplification  
514 artifacts. The model also offers interpretability through attention visualization: atten-  
515 tention weights concentrate at junction regions where template switching joins discordant  
516 loci, validating the biological relevance of the learned features. These methodological  
517 advances have direct implications for single-cell genomics, where high false-positive  
518 rates in WGA data have constrained robust characterization of chromosomal instabil-  
519 ity, clonal evolution, and SV burden [20, 22, 36]. By improving the signal-to-noise ratio  
520 and clarifying SV-type spectra that are otherwise distorted by amplification artifacts,  
521 ChimeraLM enables more confident identification of genuine SVs, supporting studies  
522 of cancer evolution, developmental biology, and somatic mosaicism where single-cell  
523 resolution is essential [26, 27].

524 Several limitations warrant consideration. First, the current model processes reads  
525 independently; integrating contextual features such as coverage or phasing informa-  
526 tion may further enhance accuracy. Second, regarding computational resources, while  
527 central processing unit (CPU) inference is feasible, graphics processing unit (GPU)  
528 acceleration is recommended for processing large-scale datasets. Finally, future work  
529 should extend validation to diverse cell types, sequencing platforms (e.g., PacBio  
530 HiFi), and alternative WGA protocols, including multiple annealing and looping-based  
531 amplification cycles (MALBAC) [37], linear amplification via transposon insertion  
532 (LIANTI) [5], primary template-directed amplification (PTA) [19], and droplet-based  
533 MDA (dMDA) [38]. While the sequence-based approach suggests broad applicability,  
534 systematic validation across amplification chemistries is needed to assess generalization  
535 limits and optimize performance for specific protocols.

536 More broadly, ChimeraLM illustrates the potential of GLMs for data qual-  
537 ity control. As long-context architectures continue to advance [29], extending the  
538 model’s context window to handle megabase-scale inputs could enable artifact detec-  
539 tion in more complex genomic structures. This framework could extend to other  
540 amplification-dependent technologies, such as cell-free DNA analysis, ancient DNA  
541 studies, and low-biomass metagenomics. Furthermore, attention-based interpretability  
542 opens opportunities for studying template-switching dynamics, potentially guiding the  
543 development of improved amplification protocols. In summary, ChimeraLM provides  
544 a practical and interpretable framework for enhancing long-read single-cell genomic  
545 fidelity, ensuring that downstream biological insights are derived from genuine SVs  
546 rather than technical artifacts.

547  
548  
549  
550  
551  
552

<b>Methods</b>	553
<b>Cell culture, single-clone preparation, and nanopore sequencing</b>	554
<i>Cell culture and single-clone establishment</i>	555
PC3 prostate cancer cells (ATCC® CRL-1435™) were cultured in RPMI-1640 medium supplemented with 10% fetal bovine serum and 1% penicillin–streptomycin at 37 °C with 5% CO <sub>2</sub> . To minimize biological heterogeneity, a monoclonal population was established by serial dilution in 96-well plates, ensuring that each culture originated from a single cell. Mycoplasma contamination was routinely tested and confirmed negative prior to DNA extraction.	556
<i>DNA extraction and whole-genome amplification</i>	557
From the monoclonal population, two types of DNA samples were prepared: a bulk (non-amplified) control and ten single-cell MDA-amplified genomes. Bulk high-molecular-weight DNA was extracted using the Monarch® HMW DNA Extraction Kit for Cells & Blood (New England Biolabs). Individual cells were isolated using 1CellDish-60 mm (iBiochips) and amplified using the REPLI-g Advanced DNA Single Cell Kit (Qiagen) following the manufacturer's protocol. DNA concentration and fragment integrity were assessed with a Qubit 4 fluorometer and Agilent TapeStation (DNA 1000/5000 ScreenTape). Only samples meeting quality standards were used for library construction.	558
<i>Nanopore library preparation and sequencing</i>	559
Libraries were prepared using the ONT Ligation Sequencing Kit V14 (SQK-LSK114) and sequenced on MinION Mk1C or PromethION P2 Solo devices with R10.4.1 flow cells following the manufacturer's genomic DNA workflow. Because all single-cell samples originated from the same monoclonal lineage, differences between amplified and bulk datasets primarily reflect MDA-induced artifacts rather than biological variation.	560
<i>Basecalling and read processing</i>	561
POD5 files were basecalled using Dorado v0.5.0 with the high-accuracy model dna_r10.4.1_e8.2_400bps_hac@v4.3.0 [39]. Reads with mean quality < 10 or length < 500 bp were removed. Adapters and concatemers were trimmed using Cutadapt v4.0 [40] in a two-pass, error-tolerant procedure. Filtered reads were aligned to the GRCh38.p13 reference genome using minimap2 v2.26 (map-ont preset) [41]. BAM files were sorted and indexed using SAMtools v1.16 [42]. Read-length and mapping statistics were computed using NanoPlot v1.46.1 [43]. All samples were processed using identical parameters.	562
<i>Chimeric read identification</i>	563
Chimeric reads were identified from BAM files using supplementary alignment (SA) tags. Reads were classified as chimeric if they (i) were mapped, (ii) contained an SA tag, (iii) were primary alignments (not secondary), and (iv) were not supplementary alignments themselves. This definition counts each chimeric read once using its primary	564
	565
	566
	567
	568
	569
	570
	571
	572
	573
	574
	575
	576
	577
	578
	579
	580
	581
	582
	583
	584
	585
	586
	587
	588
	589
	590
	591
	592
	593
	594
	595
	596
	597
	598

599 alignment while excluding secondary/supplementary records, thereby avoiding double-  
600 counting and reducing ambiguity from low-confidence alignments. Reads lacking **SA**  
601 tags were classified as non-chimeric.

602

### 603 **Training data construction**

604

#### 605 *Data generation and sources*

606 To construct the training dataset, we generated **WGA** and bulk sequencing data from  
607 PC3 cells. The **WGA** sample was amplified and sequenced on the PromethION P2 plat-  
608 form (**ONT**), while three independent bulk datasets were produced from non-amplified  
609 genomic DNA: bulk PromethION P2, bulk MinION Mk1c (**ONT**), and bulk **PacBio**.  
610 These bulk datasets represent authentic biological sequences free from amplification-  
611 induced artifacts. In contrast, **WGA** sequencing includes both genuine genomic reads  
612 and artificial chimeras introduced during the amplification process.

613

#### 614 *Ground truth annotation and class definition*

615 Ground truth labels were established by systematically comparing chimeric reads from  
616 the **WGA** PromethION P2 dataset against those from the three bulk datasets. For each  
617 **WGA** chimeric read, all alignment segments—defined by their genomic start and end  
618 coordinates—were compared to the corresponding segments of bulk chimeric reads.  
619 A **WGA** read was labeled as biological if every segment matched at least one bulk  
620 chimeric read within a 1 kb positional tolerance, indicating that the structural con-  
621 figuration is also present in non-amplified DNA. Reads lacking any matching pattern  
622 across all bulk datasets were labeled as artificial chimeras, presumed to arise from the  
623 amplification process. Additional chimeric reads were randomly sampled from the bulk  
624 datasets and labeled as biological, as these reads originate from genuine genomic rear-  
625 rangements such as true **SVs**. The final labeled dataset combined the annotated **WGA**  
626 PromethION P2 reads with the subsampled bulk chimeric reads and was subsequently  
627 partitioned into training, validation, and test sets as described below.

628

#### 629 *Dataset partitioning and cross-platform validation*

630 The combined labeled dataset, derived from **WGA** PromethION P2 and bulk sequenc-  
631 ing data, was divided into training (70%), validation (20%), and test (10%) sets using  
632 stratified random sampling. These subsets were used respectively for model training,  
633 hyperparameter tuning, and performance evaluation on data from the same sequencing  
634 platform.

635 To evaluate cross-platform generalization, the complete **WGA** MinION Mk1c  
636 dataset was reserved. This dataset, generated on a different nanopore platform,  
637 was never used during model training or internal testing. This two-level evaluation  
638 design allowed us to test whether ChimeraLM captures general sequence features of  
639 amplification-induced chimeras rather than platform-specific artifacts.

640

641

642

643

644

<b>Model architecture</b>	645
<b>DNA encoder</b>	646

ChimeraLM employs the pre-trained HyenaDNA model [29] as its DNA encoder. This model was pre-trained on large-scale genomic data and provides robust sequence representations. DNA sequences are tokenized at single-nucleotide resolution, with each base (A, C, G, T, N) mapped to a unique integer token (7, 8, 9, 10, 11, respectively). Special tokens include [CLS]=0, [PAD]=4, and others for sequence processing. Input sequences are truncated at 32,768 bp or padded to enable batch processing.

For a tokenized input sequence  $\mathbf{x} \in \mathbb{Z}^L$ , the HyenaDNA generates contextualized hidden representations:

$$\mathbf{H} = \text{HyenaDNA}(\mathbf{x}) \in \mathbb{R}^{L \times 256}$$

where  $\mathbf{H} = (\mathbf{h}_1, \mathbf{h}_2, \dots, \mathbf{h}_L)$  represents position-wise hidden states with dimension 256. The Hyena operators [33] efficiently capture both local sequence motifs and long-range dependencies essential for distinguishing biological sequences from chimeric artifacts.

### **Attention pooling**

To aggregate variable-length sequence representations into fixed-size vectors, ChimeraLM implements attention-based pooling. For hidden states  $\mathbf{H} \in \mathbb{R}^{L \times 256}$ , attention weights are computed through a two-layer network:

$$\begin{aligned} \mathbf{e} &= \text{GELU}(\text{Linear}_{256 \rightarrow 256}(\mathbf{H})) \in \mathbb{R}^{L \times 256} \\ \mathbf{s} &= \text{Linear}_{256 \rightarrow 1}(\mathbf{e}) \in \mathbb{R}^{L \times 1} \\ \boldsymbol{\alpha} &= \text{softmax}(\mathbf{s}) \in \mathbb{R}^{L \times 1} \end{aligned}$$

The pooled representation is the weighted sum of hidden states:

$$\mathbf{h}_{\text{pooled}} = \sum_{i=1}^L \alpha_i \mathbf{h}_i \in \mathbb{R}^{256}$$

This mechanism assigns learned importance weights to each sequence position, enabling the model to focus on informative regions while accommodating natural variability in read lengths.

### **Classification head**

The pooled representation is processed through a MLP with residual connections. The first layer expands dimensionality:

$$\mathbf{f}_1 = \text{Dropout}_{0.1}(\text{GELU}(\text{Linear}_{256 \rightarrow 512}(\mathbf{h}_{\text{pooled}}))) \in \mathbb{R}^{512}$$

Subsequent residual blocks with input  $\mathbf{f}_{\text{in}} \in \mathbb{R}^{512}$  compute:

$$\mathbf{f}_{\text{out}} = \text{Dropout}_{0.1}(\text{Linear}_{512 \rightarrow 512}(\text{GELU}(\text{Linear}_{512 \rightarrow 512}(\mathbf{f}_{\text{in}})))) + \mathbf{f}_{\text{in}}$$

691 where the skip connection enables stable gradient flow during training. The final layer  
692 produces binary classification logits:

693

$$694 \quad \mathbf{z} = [z_0, z_1] = \text{Linear}_{512 \rightarrow 2}(\mathbf{f}_{\text{final}}) \in \mathbb{R}^2$$

695

696 where  $z_0$  and  $z_1$  represent logits for biological and artificial chimeric classes, respec-  
697 tively. During inference, the predicted class is  $\hat{y} = \text{argmax}_{i \in \{0,1\}} z_i$ .

698

### 699 **Model summary**

700 The complete ChimeraLM pipeline processes DNA sequences through: (1) single-  
701 nucleotide tokenization, (2) HyenaDNA backbone encoding to generate contextualized  
702 representations, (3) attention pooling to aggregate position-specific features, (4) [MLP](#)  
703 layers with residual connections to learn classification features, and (5) binary clas-  
704 sification output. The entire model with  $\sim 4.2$ M trainable parameters is trained  
705 end-to-end using labeled data.

706

## 707 **Model training and optimization**

708

### 709 **Training configuration**

710 ChimeraLM was trained using PyTorch [44] and PyTorch Lightning [45] frameworks.  
711 Input sequences were tokenized using the tokenizer with maximum sequence length of  
712 32,768 bp. Sequences longer than this threshold were truncated; shorter sequences were  
713 padded to enable batch processing. Training employed mixed-precision computation  
714 (bf16) to accelerate training while maintaining numerical stability.

715

### 716 **Optimization procedure**

717 We used the AdamW optimizer [46] with learning rate  $\eta = 1 \times 10^{-4}$  and weight  
718 decay  $\lambda = 0.01$ . AdamW implements adaptive learning rates with decoupled weight  
719 decay, combining the benefits of Adam optimization with proper L2 regularization.  
720 A ReduceLROnPlateau scheduler dynamically adjusted the learning rate based on  
721 validation loss, reducing it by a factor of 0.1 when no improvement occurred for 10  
722 consecutive epochs. Early stopping with patience of 10 epochs prevented overfitting  
723 by terminating training when validation performance plateaued. A fixed random seed  
724 (12345) ensured reproducibility across training runs.

725 The training objective used cross-entropy loss for binary classification. For a  
726 training example with class label  $y \in \{0, 1\}$  and model logits  $\mathbf{z} = [z_0, z_1]$ , the loss is:

727

$$728 \quad \mathcal{L}(\mathbf{z}, y) = -\log \left( \frac{\exp(z_y)}{\exp(z_0) + \exp(z_1)} \right) = -z_y + \log(\exp(z_0) + \exp(z_1))$$

729

730

731 where  $z_0$  and  $z_1$  represent logits for biological and artificial chimeric classes, respec-  
732 tively.

733

### 734 **Training implementation**

735 Training used batch size of 16 sequences with 30 parallel data loading workers. [GPU](#)  
736 acceleration was employed for efficient processing, with training typically requiring

55 hours. Model checkpointing saved the best-performing model based on validation metrics. Configuration management used Hydra [47] to enable reproducible experimentation.

### ***Model evaluation***

Performance was monitored using precision, recall, and F1 score on the validation set after each epoch:

$$\text{Precision} = \frac{\text{TP}}{\text{TP} + \text{FP}}, \quad \text{Recall} = \frac{\text{TP}}{\text{TP} + \text{FN}}$$
$$\text{F1} = \frac{2 \times \text{Precision} \times \text{Recall}}{\text{Precision} + \text{Recall}}$$

where TP (true positives) are chimeric reads correctly classified as artificial, TN (true negatives) are biological reads correctly classified as biological, FP (false positives) are biological reads misclassified as artificial, and FN (false negatives) are artificial reads misclassified as biological. Final model selection was based on best validation performance as determined by early stopping.

## **Model inference and application**

### ***Inference pipeline***

To apply ChimeraLM to new WGA sequencing data, the model takes a BAM file as input. Chimeric reads are identified using SA tags and filtered to exclude unmapped, secondary, or supplementary alignments. Each chimeric read sequence is tokenized using the tokenizer (maximum length 32,768 bp, with truncation or padding as needed). The trained model processes sequences in batches, generating two logits  $[z_0, z_1]$  for each read corresponding to biological and artificial chimeric classes. Classification is determined by  $\hat{y} = \text{argmax}(z_0, z_1)$ . ChimeraLM outputs a filtered BAM file containing only reads classified as biological, which can be directly used for downstream analyses including SV calling.

## **Performance evaluation**

### ***Test set evaluation***

Final model performance was evaluated on the held-out test set and the independent MinION Mk1c dataset. Metrics (precision, recall, and F1 score) were computed as described in the training section, where true positives represent chimeric reads correctly classified as artificial and true negatives represent biological reads correctly classified as biological.

### ***SV calling***

SVs were called using multiple tools to ensure comprehensive detection. For long-read data (ONT PromethION P2 and MinION Mk1c), we used Sniffles v2.5 [14, 15], DeBreak v1.2 [16], SVIM v2.0.0 [17], and cuteSV v2.1.1 [18]. For short-read data of the PC3 cell line, we used both the CCLE Illumina WGS dataset and the PRJNA361315

783 Illumina **WGS** dataset, processed with Manta v1.6.0 [48], DELLY v1.5.0 [49], and  
784 SvABA v1.1.0 [50]. All tools were executed with default recommended parameters.

785

#### 786 ***Gold standard SV dataset construction***

787 To evaluate the impact of ChimeraLM on **SV** detection accuracy, we generated a high-  
788 confidence gold-standard **SV** set from bulk PC3 sequencing data. All **SV** comparisons  
789 and breakpoint corrections were performed using OctopuSV v0.2.3 [51]. Four bulk  
790 datasets were integrated: **ONT** MinION Mk1c, **ONT** PromethION P2, the CCLE Illumina  
791 **WGS** dataset, and the PRJNA361315 Illumina **WGS** dataset. **SVs** were called  
792 independently within each dataset, and events supported by at least two **SV** callers  
793 were retained. The remaining calls were then compared across datasets, and **SVs**  
794 observed in at least two of the four datasets were designated as gold-standard events  
795 for benchmarking.

796

#### 797 ***SV benchmarking analysis***

798 To assess the impact of ChimeraLM on **SV** calling accuracy, we compared **SV** calls from  
799 unfiltered **WGA** data and ChimeraLM-filtered **WGA** data against two references: (1)  
800 the stringent multi-platform gold standard dataset, and (2) platform-matched long-  
801 read bulk sequencing data. Benchmarking was performed using Truvari v4.2.2 [52]  
802 with default parameters. **SVs** were considered supported if they matched reference  
803 variants within the defined breakpoint tolerance. Validation rates were calculated as  
804 the proportion of called **SVs** supported by the reference. This dual benchmarking  
805 strategy quantifies both improvements in detecting high-confidence multi-platform  
806 **SVs** and the retention of platform-specific true variants.

807

### 808 **Benchmarking against existing methods**

809 ChimeraLM was compared to existing computational methods for detecting  
810 amplification-induced chimeric artifacts: SACRA [25] (GitHub commit 9a2607e), 3rd-  
811 ChimeraMiner [13] (GitHub commit 04b5233), and CADECT v1.2 [11]. Both tools  
812 were applied to **WGA** data from PromethION P2 and MinION Mk1c platforms using  
813 default parameters as recommended in their documentation. Performance was evalua-  
814 ted by measuring the percentage reduction in chimeric reads relative to unprocessed  
815 **WGA** data. Chimeric reads were identified using **WGA** tag-based alignment criteria  
816 (reads with **SA** tags indicating split alignments), and reduction rates were calculated  
817 as the proportion of chimeric reads removed by each method.

818

### 819 **Attention weight analysis**

820

821 To investigate ChimeraLM's interpretability, we analyzed attention weights from  
822 the pooling mechanism for representative chimeric reads. Attention weights indicate  
823 the relative importance assigned to each sequence position during classification. For  
824 selected reads, we extracted per-position attention weights and visualized them along-  
825 side read alignments to identify whether the model focuses on mechanistically relevant  
826 regions.

827

828

Chimeric junction positions were identified from alignment data (defined by break-points in SA tags). A region of  $\pm 50$  bp surrounding each junction was designated as the junction region. Attention weights within junction region were compared to non-junction regions using the Wilcoxon rank-sum test [53], with statistical significance assessed at  $p < 0.001$ . 829  
830  
831  
832  
833  
834

## Data visualization

Figures were generated using Python with Matplotlib [54] and Seaborn [55]. 835  
836  
837

## Computing resources

Computations were performed on a high performance computing (HPC) server with 64-core Intel Xeon Gold 6338 CPU, 256 GB RAM, and two NVIDIA A100 GPUs (80 GB memory each). 838  
839  
840  
841  
842  
843  
844  
845

**Extended Data Table 1** Sequencing and alignment statistics of PC3

Sample	Platform	Reads ( $\times 10^6$ )	Total bases (Gb)	Total bases aligned (Gb)	Fraction aligned	Mean length (bp)	Mean quality (Q)	Average identity (%)
WGA	MinION	9.11	14.6	10.4	0.7	1,603	14.3	97.6
WGA	PromethION	44.69	128.2	69.2	0.5	2,869	14.5	96.1
Bulk	MinION	0.97	8.1	7.1	0.9	8,310	17.2	97.3
Bulk	PromethION	8.00	69.9	62.4	0.9	8,732	18.5	97.7

## Supplementary information.

875

876

877

878

879

880

881

882

883

884

885

886

887

888

889

890

891

892

893

894

895

896

897

898

899

900

**901 Extended Data Fig. 1 Training dataset construction and bulk-supported labeling strat-  
902 egy.** (a) Workflow for generating labeled training data. **WGA** PromethION data is compared against  
903 three independent bulk sequencing datasets (PromethION, MinION, and PacBio). Reads with no  
904 bulk matches (Match 0) are labeled artificial; reads matching one or more bulk datasets (Match 1–3)  
905 are labeled biological, along with chimeric reads sampled directly from bulk data. The labeled dataset  
906 is split into training (70%), validation (20%), and test (10%) sets. The **WGA** MinION dataset is  
907 reserved for independent cross-platform evaluation. (b) Distribution of chimeric read matches. Bar  
908 chart shows the number of **WGA** PromethION chimeric reads (log scale) by bulk dataset matches.  
909 Match 0 reads ( $\sim 10^7$ ) lacking bulk validation are classified as artificial; Match 1–3 reads with bulk sup-  
910 port are classified as biological. The substantial imbalance reflects high prevalence of **WGA**-induced  
911 artifacts.

912

913

914

915

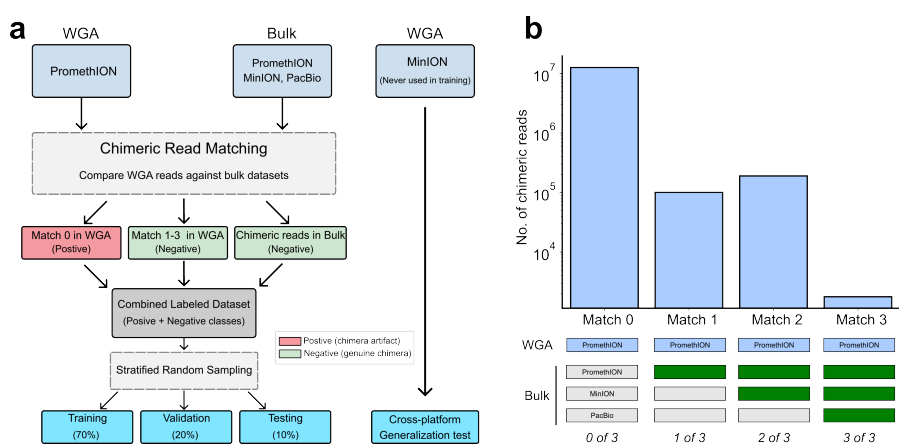
916

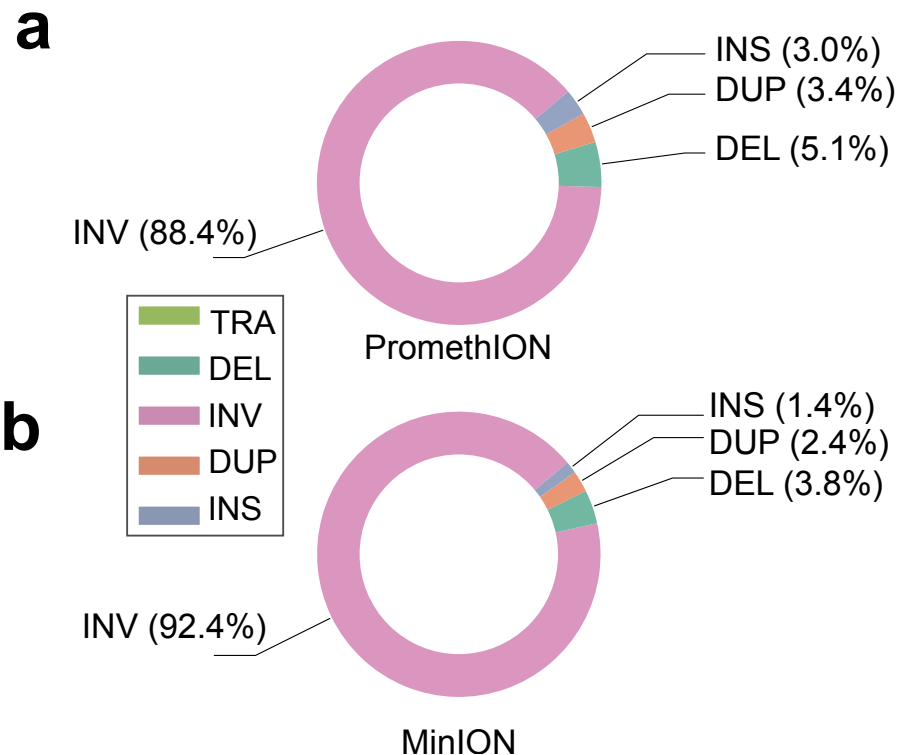
917

918

919

920





**Extended Data Fig. 2** Composition of artifact-supported **SVs** for PromethION (a) and MinION (b). Donut charts summarize **SV** types among events supported exclusively by chimeric reads, representing artificial **SVs** preferentially removed by ChimeraLM.

921  
922  
923  
924  
925  
926  
927  
928  
929  
930  
931  
932  
933  
934  
935  
936  
937  
938  
939  
940  
941  
942  
943  
944  
945  
946  
947  
948  
949  
950  
951  
952  
953  
954  
955  
956  
957  
958  
959  
960  
961  
962  
963  
964  
965  
966

967 **Acknowledgements.** We thank Tingyou Wang for guidance on figure preparation.  
968 This project was supported in part by NIH grants R35GM142441 and R01CA259388  
969 awarded to RY.

970

## 971 **Declarations**

972

973 **Author Contributions.** YL, QG and RY designed the study. YL and QG per-  
974 formed the analysis. QG performed the experiments. YL and QG designed and  
975 implemented the model. YL built the command-line tool and documentation. YL, QG  
976 and RY wrote the manuscript. RY supervised this work.

977

978 **Data Availability.** The raw sequencing data generated in this study have been  
979 deposited in the NCBI Sequence Read Archive (SRA) under BioProject accession  
980 PRJNA1354861. The dataset includes Oxford Nanopore long-read whole-genome  
981 sequencing of PC3 prostate cancer cells and MDA-amplified single-cell derivatives. The  
982 individual SRA accessions are as follows: PC3 bulk (MinION Mk1C), SRR35904028;  
983 PC3 bulk (PromethION P2), SRR35904029; PC3 10-cell WGA (MinION Mk1C),  
984 SRR35904026; PC3 10-cell WGA (PromethION P2), SRR35904027. We can access the  
985 data at the following link: <https://dataview.ncbi.nlm.nih.gov/object/PRJNA1354861?reviewer=viej6cv6mgbli3n7a9a5k1bsb3>

986

987 **Code Availability.** ChimeraLM, implemented in Python, is open source and  
988 available on GitHub (<https://github.com/ylab-hi/ChimeraLM>) under the Apache  
989 License, Version 2.0. The package can be installed via PyPI (<https://pypi.org/project/chimeralm>) using pip, with wheel distributions provided for Windows, Linux, and  
990 macOS to ensure easy cross-platform installation. An interactive demo is available on  
991 Hugging Face (<https://huggingface.co/spaces/yangliz5/ChimeraLM>), allowing users  
992 to test ChimeraLM's functionality without local installation. For large-scale analy-  
993 ses, we recommend using ChimeraLM on systems with GPU acceleration. Detailed  
994 system requirements and optimization guidelines are available in the repository's  
995 documentation (<https://ylab-hi.github.io/ChimeraLM/>).

996

997 **Conflict of interest.** RY has served as an advisor/consultant for Tempus AI, Inc.  
998 This relationship is unrelated to and did not influence the research presented in this  
999 study.

1000

## 1001 **Acronyms**

1002

1003 **CPU** central processing unit 12

1004

1005 **DEL** deletion 8, 9

1006 **dMDA** droplet-based MDA 12

1007 **DUP** duplication 8, 9

1008

1009 **GLM** genomic language model 1, 2, 12

1010 **GPU** graphics processing unit 12, 16, 19, 22

1011

1012 **HPC** high performance computing 19

<b>INS</b> insertion	8, 9	1013
<b>INV</b> inversion	2, 7–10	1014
		1015
<b>LIANTI</b> linear amplification via transposon insertion	12	1016
<b>MALBAC</b> multiple annealing and looping-based amplification cycles	12	1017
<b>MDA</b> multiple displacement amplification	2	1018
<b>MLP</b> multilayer perceptron	4, 5, 15, 16	1019
<b>ONT</b> Oxford Nanopore Technologies	3, 7, 8, 11, 13, 14, 17, 18	1020
<b>PacBio</b> Pacific Biosciences	3, 14	1021
<b>PTA</b> primary template-directed amplification	12	1022
<b>SA</b> supplementary alignment	13, 14, 17–19	1023
<b>SV</b> structural variation	1–4, 6–9, 11, 12, 14, 17, 18, 21	1024
<b>TRA</b> translocation	2, 8	1025
<b>WGA</b> whole genome amplification	1–12, 14, 17–20	1026
<b>WGS</b> whole genome sequencing	7, 8, 17, 18	1027
		1028
<b>References</b>		1029
[1] Kalf-Ezra, E. <i>et al.</i> Single-cell somatic copy number variants in brain using different amplification methods and reference genomes. <i>Communications Biology</i> 1288 (2024).		1030
[2] Navin, N. <i>et al.</i> Tumour evolution inferred by single-cell sequencing. <i>Nature</i> <b>472</b> , 90–94 (2011).		1031
[3] Sun, C. <i>et al.</i> Mapping recurrent mosaic copy number variation in human neurons. <i>Nature Communications</i> 4220 (2024).		1032
[4] Gawad, C., Koh, W. & Quake, S. R. Single-cell genome sequencing: current state of the science. <i>Nature Reviews Genetics</i> 175–188 (2016).		1033
[5] Chen, C. <i>et al.</i> Single-cell whole-genome analyses by linear amplification via transposon insertion (LIANTI). <i>Science (new York, N.Y.)</i> <b>356</b> , 189–194 (2017).		1034
[6] Macaulay, I. C. & Voet, T. Single cell genomics: Advances and future perspectives. <i>PLOS Genetics</i> <b>10</b> , e1004126 (2014).		1035
[7] de Bourcy, C. F. A. <i>et al.</i> A quantitative comparison of single-cell whole genome amplification methods. <i>PLoS ONE</i> e105585 (2014).		1036
[8] Biezuner, T. <i>et al.</i> Comparison of seven single cell whole genome amplification commercial kits using targeted sequencing. <i>Scientific Reports</i> 17171 (2021).		1037
		1038
		1039
		1040
		1041
		1042
		1043
		1044
		1045
		1046
		1047
		1048
		1049
		1050
		1051
		1052
		1053
		1054
		1055
		1056
		1057
		1058

- 1059 [9] Lu, N., Qiao, Y., Lu, Z. & Tu, J. Chimera: The spoiler in multiple displacement  
1060 amplification. *Computational and Structural Biotechnology Journal* 1688–1696  
1061 (2023).
- 1062
- 1063 [10] Lasken, R. S. & Stockwell, T. B. Mechanism of chimera formation during the  
1064 multiple displacement amplification reaction. *BMC Biotechnology* **7**, 19 (2007).
- 1065
- 1066 [11] Agyabeng-Dadzie, F. *et al.* Evaluating the benefits and limits of multiple displace-  
1067 ment amplification with whole-genome oxford nanopore sequencing. *Molecular*  
1068 *Ecology Resources* e14094 (2025).
- 1069
- 1070 [12] Dean, F. B. *et al.* Comprehensive human genome amplification using multiple  
1071 displacement amplification. *Proceedings of the National Academy of Sciences* **99**,  
1072 5261–5266 (2002).
- 1073
- 1074 [13] Lu, N. *et al.* Exploration of whole genome amplification generated chimeric  
1075 sequences in long-read sequencing data. *Briefings in Bioinformatics* **24**, bbad275  
1076 (2023).
- 1077
- 1078 [14] Sedlazeck, F. J. *et al.* Accurate detection of complex structural variations using  
1079 single-molecule sequencing. *Nature Methods* 461–468 (2018).
- 1080
- 1081 [15] Smolka, M. *et al.* Detection of mosaic and population-level structural variants  
1082 with sniffles2. *Nature Biotechnology* 1571–1580 (2024).
- 1083
- 1084 [16] Chen, Y. *et al.* Deciphering the exact breakpoints of structural variations using  
1085 long sequencing reads with DeBreak. *Nature Communications* 283 (2023).
- 1086
- 1087 [17] Heller, D. & Vingron, M. SVIM: Structural variant identification using mapped  
1088 long reads. *Bioinformatics* 2907–2915 (2019).
- 1089
- 1090 [18] Jiang, T. *et al.* Long-read-based human genomic structural variation detection  
1091 with cuteSV. *Genome Biology* 189 (2020).
- 1092
- 1093 [19] Gonzalez-Pena, V. *et al.* Accurate genomic variant detection in single cells with  
1094 primary template-directed amplification. *Proceedings of the National Academy of*  
1095 *Sciences* **118**, e2024176118 (2021).
- 1096
- 1097 [20] Kosugi, S. *et al.* Comprehensive evaluation of structural variation detection  
1098 algorithms for whole genome sequencing. *Genome Biology* **20**, 117 (2019).
- 1099
- 1100 [21] Alkan, C., Coe, B. P. & Eichler, E. E. Genome structural variation discovery and  
1101 genotyping. *Nature Reviews Genetics* **12**, 363–376 (2011).
- 1102
- 1103 [22] Hård, J. *et al.* Long-read whole-genome analysis of human single cells. *Nature*  
1104 *Communications* **14**, 5164 (2023).

- [23] Gupta, P., O'Neill, H., Wolvetang, E. J., Chatterjee, A. & Gupta, I. Advances in single-cell long-read sequencing technologies. *NAR Genomics and Bioinformatics* **6**, lqae047 (2024). 1105  
1106  
1107  
1108  
1109  
1110  
1111  
1112  
1113  
1114  
1115  
1116  
1117  
1118
- [24] Wen, L. & Tang, F. Single-cell omics sequencing technologies: The long-read generation. *Trends in Genetics* **0** (2025). 1119  
1120  
1121
- [25] Kiguchi, Y., Nishijima, S., Kumar, N., Hattori, M. & Suda, W. Long-read metagenomics of multiple displacement amplified DNA of low-biomass human gut phageomes by SACRA pre-processing chimeric reads. *DNA Research* **28**, dsab019 (2021). 1122  
1123  
1124  
1125  
1126  
1127  
1128
- [26] Ha, Y.-J. *et al.* Comprehensive benchmarking and guidelines of mosaic variant calling strategies. *Nature Methods* **20**, 2058–2067 (2023). 1129  
1130  
1131  
1132  
1133  
1134  
1135  
1136  
1137  
1138  
1139
- [27] Höijer, I. *et al.* Amplification-free long-read sequencing reveals unforeseen CRISPR-Cas9 off-target activity. *Genome Biology* **21**, 290 (2020). 1140  
1141  
1142  
1143  
1144  
1145  
1146  
1147  
1148  
1149  
1150
- [28] Li, Y. *et al.* A genomic language model for chimera artifact detection in nanopore direct rna sequencing. *bioRxiv* (2024). URL <https://www.biorxiv.org/content/early/2024/10/25/2024.10.23.619929>. 1140  
1141  
1142  
1143  
1144  
1145  
1146  
1147  
1148  
1149  
1150
- [29] Nguyen, E. *et al.* *HyenaDNA: Long-range genomic sequence modeling at single nucleotide resolution*, Vol. 36, 43177–43201 (Curran Associates, Inc., 2023). 1140  
1141  
1142  
1143  
1144  
1145  
1146  
1147  
1148  
1149  
1150
- [30] Dalla-Torre, H. *et al.* Nucleotide transformer: building and evaluating robust foundation models for human genomics. *Nature Methods* 287–297 (2025). 1140  
1141  
1142  
1143  
1144  
1145  
1146  
1147  
1148  
1149  
1150
- [31] Zhou, Z. *et al.* *DNABERT-2: Efficient foundation model and benchmark for multi-species genomes*, 1–24 (OpenReview.net, 2024). 1140  
1141  
1142  
1143  
1144  
1145  
1146  
1147  
1148  
1149  
1150
- [32] Consens, M. E. *et al.* To transformers and beyond: Large language models for the genome (2023). [arXiv:2311.07621](https://arxiv.org/abs/2311.07621). 1140  
1141  
1142  
1143  
1144  
1145  
1146  
1147  
1148  
1149  
1150
- [33] Poli, M. *et al.* *Hyena hierarchy: Towards larger convolutional language models*, Vol. 202, 28043–28078 (PMLR, 2023). 1140  
1141  
1142  
1143  
1144  
1145  
1146  
1147  
1148  
1149  
1150
- [34] Barretina, J. *et al.* The Cancer Cell Line Encyclopedia enables predictive modelling of anticancer drug sensitivity. *Nature* **483**, 603–607 (2012). 1140  
1141  
1142  
1143  
1144  
1145  
1146  
1147  
1148  
1149  
1150
- [35] Seim, I., Jeffery, P. L., Thomas, P. B., Nelson, C. C. & Chopin, L. K. Whole-Genome Sequence of the Metastatic PC3 and LNCaP Human Prostate Cancer Cell Lines. *G3 (Bethesda, Md.)* **7**, 1731–1741 (2017). 1140  
1141  
1142  
1143  
1144  
1145  
1146  
1147  
1148  
1149  
1150
- [36] Mahmoud, M. *et al.* Structural variant calling: The long and the short of it. *Genome Biology* **20**, 246 (2019). 1140  
1141  
1142  
1143  
1144  
1145  
1146  
1147  
1148  
1149  
1150

- 1151 [37] Zong, C., Lu, S., Chapman, A. R. & Xie, X. S. Genome-wide detection of single-  
1152 nucleotide and copy-number variations of a single human cell. *Science* 1622–1626  
1153 (2012).
- 1154
- 1155 [38] Dippenaar, A. *et al.* Droplet based whole genome amplification for sequencing  
1156 minute amounts of purified mycobacterium tuberculosis DNA. *Scientific Reports*  
1157 14, 9931 (2024).
- 1158
- 1159 [39] PLC., O. N. Dorado. <https://github.com/nanoporetech/dorado> (2023).
- 1160
- 1161 [40] Martin, M. Cutadapt removes adapter sequences from high-throughput sequenc-  
1162 ing reads. *Embnet.journal* 17, 10–12 (2011).
- 1163
- 1164 [41] Li, H. Minimap2: Pairwise alignment for nucleotide sequences. *Bioinformatics*  
1165 3094–3100 (2018).
- 1166
- 1167 [42] Danecek, P. *et al.* Twelve years of SAMtools and BCFtools. *GigaScience* giab008  
1168 (2021).
- 1169
- 1170 [43] De Coster, W. & Rademakers, R. NanoPack2: Population-scale evaluation of  
1171 long-read sequencing data. *Bioinformatics* 39, btad311 (2023).
- 1172
- 1173 [44] Paszke, A. *et al.* PyTorch: An imperative style, high-performance deep learning  
1174 library, Vol. 32, 8024–8035 (Curran Associates, Inc., 2019).
- 1175
- 1176 [45] Falcon, W. & The PyTorch Lightning team. PyTorch Lightning. GitHub  
1177 repository (2019). URL <https://github.com/Lightning-AI/lightning>.
- 1178
- 1179 [46] Loshchilov, I. & Hutter, F. Decoupled weight decay regularization (2019).
- 1180
- 1181 [47] Yadan, O. Hydra - a framework for elegantly configuring complex applications.  
GitHub repository (2019). URL <https://github.com/facebookresearch/hydra>.
- 1182
- 1183 [48] Chen, X. *et al.* Manta: Rapid detection of structural variants and indels for  
1184 germline and cancer sequencing applications. *Bioinformatics* 1220–1222 (2016).
- 1185
- 1186 [49] Rausch, T. *et al.* DELLY: Structural variant discovery by integrated paired-end  
1187 and split-read analysis. *Bioinformatics* i333–i339 (2012).
- 1188
- 1189 [50] Wala, J. A. *et al.* SvABA: Genome-wide detection of structural variants and  
1190 indels by local assembly. *Genome Research* 581–591 (2018).
- 1191
- 1192 [51] Guo, Q., Li, Y., Wang, T.-Y., Ramakrishnan, A. & Yang, R. OctopusV and  
1193 TentacleSV: A one-stop toolkit for multi-sample, cross-platform structural variant  
1194 comparison and analysis. *Bioinformatics* btaf599 (2025).
- 1195
- 1196 [52] English, A. C., Menon, V. K., Gibbs, R. A., Metcalf, G. A. & Sedlazeck, F. J.  
Truvari: Refined structural variant comparison preserves allelic diversity. *Genome*

<i>Biology</i> <b>23</b> , 271 (2022).	1197
	1198
[53] Virtanen, P. <i>et al.</i> SciPy 1.0: Fundamental algorithms for scientific computing in python. <i>Nature Methods</i> 261–272 (2020).	1199
	1200
	1201
[54] Hunter, J. D. Matplotlib: A 2d graphics environment. <i>Computing in Science &amp; Engineering</i> 90–95 (2007).	1202
	1203
[55] Waskom, M. L. seaborn: statistical data visualization. <i>Journal of Open Source Software</i> 3021 (2021).	1204
	1205
	1206
	1207
	1208
	1209
	1210
	1211
	1212
	1213
	1214
	1215
	1216
	1217
	1218
	1219
	1220
	1221
	1222
	1223
	1224
	1225
	1226
	1227
	1228
	1229
	1230
	1231
	1232
	1233
	1234
	1235
	1236
	1237
	1238
	1239
	1240
	1241
	1242